Study on Morphology Evolution, Orientational Behavior, and Anisotropic Phase Formation of Highly Filled Polymer-Layered Silicate Nanocomposites

Chong Min Koo,[†] Sang Ouk Kim,[‡] and In Jae Chung*[,†]

Applied Rheology Laboratory, Department of Chemical and Biomolecular Engineering, Korea Advanced Institute of Science and Technology, 373−1, Kusong-dong, Yusong-gu, Taejon 305−701, South Korea, and Department of Chemical Engineering, University of Wisconsin−Madison, 2020 Engineering Hall, 1415 Engineering Drive, Madison, Wisconsin 53706-1691

Received August 22, 2002

ABSTRACT: Morphology evolution, anisotropic phase behavior, and orientational behaviors of the highly filled polymer-organically modified layered silicate nanocomposites are investigated by using synchrotron small-angle X-ray scattering (SAXS), transmission electron microscopy (TEM) and polarized light microscopy (PLM). Two kinds of polymers, maleated polypropylene and maleated polyethylene were used as a matrix polymer. The final morphology of both polymer-organically modified layered silicate nanocomposites evolves via four stages; intercalation, dual states of intercalation and exfoliation, ordered exfoliation, and disordered exfoliation in sequence as the concentration of silicate decreases in the nanocomposites. The morphology evolution of nanocomposites is determined by balancing an interaction between polymer and silicate against interactions between silicate platelets such as a steric interaction and an attractive interaction, which depends on the concentration of silicates. Both the nanocomposites show the optical anisotropy above 12 vol % clay originating from the ordering of silicate layers. The layered silicates subjected to shear flow show the orientation behavior that the silicate platelet's normals are perpendicular to the flow direction. Degree of orientational order changes with the concentration as well as shear rate in a complex manner. Up to an intermediate concentration, the extent of order is enhanced with the clay concentration. In contrast, at high concentrations, the extent of order decreases or increases according to the type of nanocomposite. The differences are discussed through the consideration of the morphology, the particle−particle interaction, and the rheological property of the nanocomposites.

Introduction

Polymer-layered silicate nanocomposites (PLSNs) have attracted a great attention due to their academic and industrial importance. They have shown dramatic improvements in mechanical, thermal, and barrier properties with a small amount of inorganic layered silicate.[1−9] Moreover, they give a model system for the studies not only on the polymer chain dynamics in the confined geometry[10−18] but also on the phase behavior of polymer-nanoparticle mixture.[19−31]

From the structural point of view, two types of PLSNs are possible. The *intercalated* structure is well-ordered multilayered structures where the extended polymer chains are inserted into the gallery space between the individual silicate layers. The *exfoliated* structure results when the individual silicate layers are no longer close enough to interact with the adjacent layers.

From the processing and application points of view, it is important to understand rheological behavior as well as the orientational behavior of the nanocomposites containing highly anisometric silicates. A lot of studies on PLSNs have shown a significant change in the viscoelastic property depending not only on their morphology but also on the interfacial characteristics between polymer and layered silicate.[13−18] However, the orientational behavior of nanocomposites relating to their morphologies and their concentrations of silicate have been less well investigated, especially in a highly filled system. In general, it is known that the different interactions between the particles such as a steric interaction and long-range interaction, and the changes in concentration of particles produce a variety of microstructure and orientation behavior at different shear rates.[32,33]

The previous article showed that the microstructure of silicate layers in PLSNs evolutes through distinct four steps (intercalation, dual states of exfoliation and intercalation, ordered exfoliation, and disordered exfoliation), which are determined by balancing an interaction between polymer and silicate against interactions between silicate platelets such as attractive interaction and steric interaction.[31]At the high concentration of silicate, final morphology of silicate layers is dominated by strong attractive interaction (e.g., van der Waals interaction) between adjacent silicate layers because the interlayer distance between adjacent silicate layers are so close to interact strongly by van der Waals interaction. At the intermediate concentration of silicate, the morphology is dominated by the steric interaction rather than attractive interaction because the interdistance between adjacent silicate layers is too long for them to interact with one another by van der Waals interaction and close enough to interact by steric interaction. At the low concentration of silicate, the morphology is not governed by interactions between silicate layers because an interaction between a polymer and layered silicates overwhelms interactions between adjacent silicate layers.

* Corresponding author. E-mail: chung@kaist.ac.kr. Telephone: +82-42-869-3916. Fax: +82−42−869−3910.
[†] Korea Advanced Institute of Science and Technology.
[‡] University of Wisconsin−Madison.

10.1021/ma021377n CCC: $25.00
Published on Web 03/26/2003

Table 1. Characterization of Maleated Polyethylene (MAPE) and Maleated Polypropylene (MAPP)

	M_w[a]	PDI (M_w/M_n)[a]	T_m (°C)[b]	MA content[c] (wt %)
MAPP	59 000	2.3	156.9	1.9
MAPE	9300	2.1	99.2	3.0

[a] Measured by GPC. [b] Measured by DSC at the 10 °C/min heating. [c] Measured by elemental analysis.

In this work, a maleated polyethylene (MAPE)/organically modified montmorillonite nanocomposite and a maleated polypropylene (MAPP)/organically modified montmorillonite nanocomposite prepared by the melt intercalation method are used as a model system. We investigate the morphology evolution, orientational behavior, and anisotropic phase behavior of both nanocomposites by using SAXS, TEM, and PLM. The morphology of both nanocomposites changing with concentration of silicates is investigated by the considering an interaction between polymer and silicate and interactions between silicate platelets. We investigate how the optical anisotropy and shear-induced orientation behavior are highly related with the morphology of layered silicate in the nanocomposites. In particular, the complex shear-induced orientation behaviors of the silicates in the nanocomposites are discussed through the consideration of morphology, particle−particle interactions, and rheological properties of the nanocomposites.

Experimental Section

Materials. Maleated polyethylene (MAPE) and maleated polypropylene (MAPP) were obtained from Aldrich Co. and Honam Chem. Co., respectively. The basic characteristics of MAPE and MAPP used in this study are summarized in Table 1. To overcome the limitation in processing and high elasticity of highly loaded nanocomposites, MAPE and MAPP with a low molecular weight are used. Organophilic montmorillonite (Cloisite 20A, abbreviation 20A) was purchased from Southern Clay, which was known to be ion-exchanged with dimethyl dihydrogenated tallow ammonium ions. 20A contained an organic modifier of about 30 wt %, which was measured by TGA. The specific gravity of 20A measured by pycnometer was 1.8 g/mL. MAPE/20A and MAPP/20A nanocomposites were prepared by the melt intercalation method. Each polymer was mechanically mixed with 20A for 20 min in a Brabender mixer at 160 and 190 °C, respectively. For the investigation of the shear-induced orientational behavior, the nanocomposite fibers were made by the extrusion through capillary of a viscometer (Rosand RH5).

Characterization. The periodic structure and the orientational behavior of silicate layers in the nanocomposites were evaluated by the synchrotron SAXS at the Pohang Light Source (PLS) in Pohang, Korea, which can detect between about 0.2 and 5°. We just named this X-ray diffraction as SAXS due to including quite a small angle region. SAXS measurements were performed with point focusing (0.2 × 0.2 mm) at the 4C1 X-ray beamline of the Pohang Light Source (PLS). One-dimensional (1-D) SAXS patterns were obtained from a diode-array positional sensitive detector with a wavelength of 1.608 Å. A beam path was maintained under a vacuum to reduce air scattering, and tungsten foil (50 μm) was used for primary beam protection. A Kapton film window (7 μm thick) was used to contain samples in the melt state. The measured intensity was corrected for background scattering, a detector noise and absorption by the sample. Two-dimensional (2-D) SAXS patterns were recorded in imaging plates and read out with scanner (MAC Science). The distance between the sample and detector (or imaging plate) was 600 mm. For the TEM observation, thin films of the nanocomposites were prepared by cryogenic ultramicrotoming (RMC MT7000) at −120 °C.

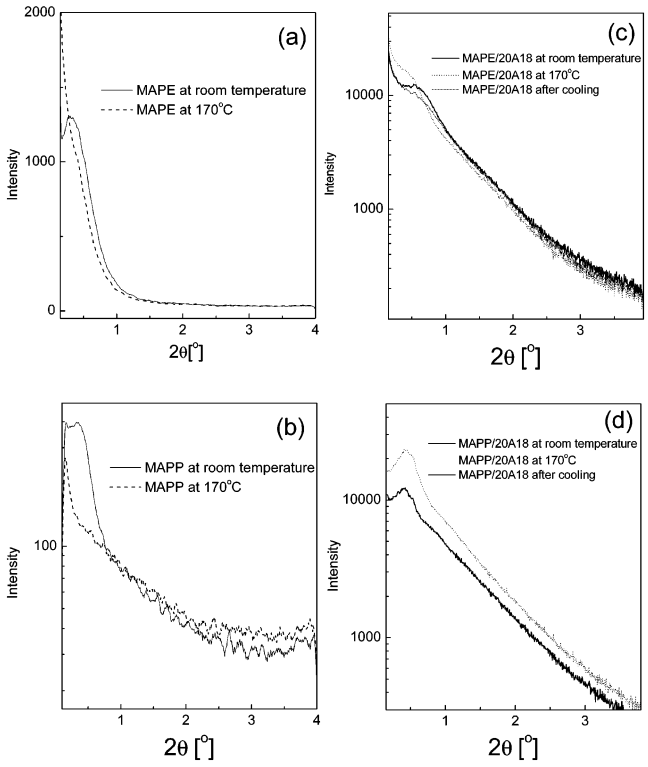

Figure 1. SAXS patterns of (a) MAPE, (b) MAPP, (c) MAPE/20A18 fiber, and (d) MAPP/20A18 fiber at room temperature and above melting temperature of matrix polymer.

These films were observed by TEM (Philips CM-20 transmission electron microscope). Viscoelastic properties were conducted with ARES, strain-controlled rheometer. A cone and plate with a diameter of 50 mm was used. All test were performed in the linear viscoelastic region. The birefringence was studied by a polarized light microscopy (PLM, A Leitz, model Laborlux 12 Pols) coupled with a Mettler FP-2 hot stage. In order to minimize the history of sample preparation, MAPP/20A nanocomposites on the slide glass were squeezed very slowly with a cover glass at 200 °C.

Results and Discussion

Morphology Evolution of the Nanocomposites. Figure 1 shows SAXS patterns of MAPE, MAPP, MAPE/20A18 fiber, and MAPP/20A18 fiber at room temperature and above the melting temperature of the matrix polymer. The nanocomposite fibers were scanned in the equatorial direction of the fiber axis. The number following MAPE/20A stands for the volume percent of organically modified silicate, 20A. In Figure 1, parts a and b, pure MAPE and MAPP have the basal plane peak around 0.5° at room temperature, not above the melting temperature. The peaks must be from the lamellae thickness of each polymer. In contrast, MAPE/20A18 and MAPP20A18 show the basal plane peak below 1° not only at the room temperature but also above the melting temperature. It indicates that the peak in the nanocomposites must be originated from the (001) reflection peak of layered silicate. It seems that the scattering of matrix polymer is weak enough to be negligible compared with the scattering of the silicate layers in the highly filled nanocomposites. The peak position of MAPE/20A18 moves toward a quite lower angle on heating and returns to its original position on cooling. Peak intensity reduces during this heat treatment. The peak shift toward a lower angle in MAPE/20A during heating may be due to the thermal expan-

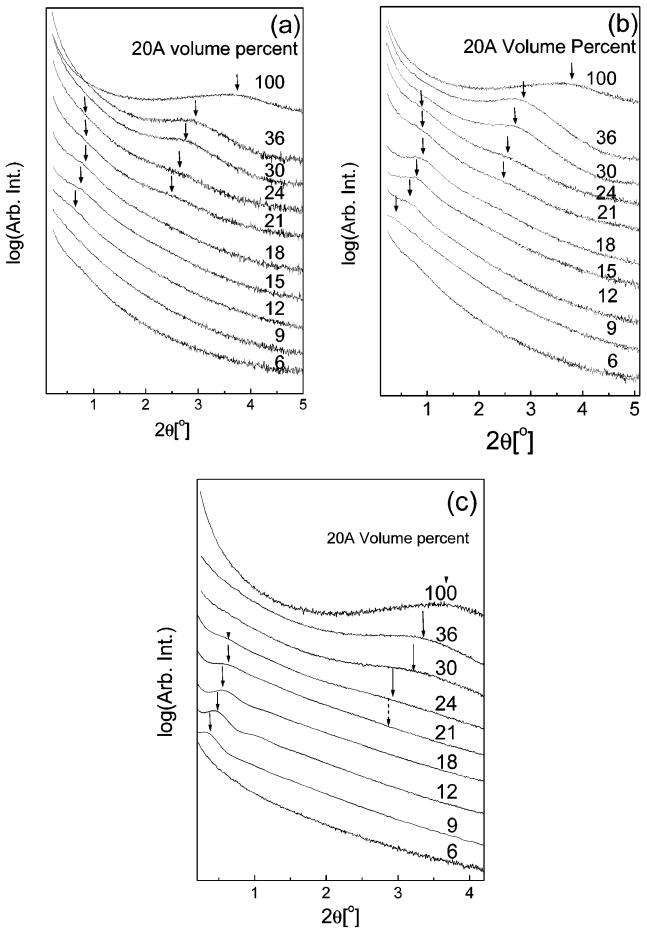

Figure 2. SAXS patterns of (a) as-mixed MAPE/20A nanocomposites, (b) extruded MAPE/20A nanocomposite fibers, and (c) extruded MAPP/20A nanocomposite fibers with the different amounts of clay. The nanocomposite fibers extruded by a capillary viscometer were scanned in the equatorial direction of fiber axis.

sion of polymer existing between silicate layers. The reduction of the peak intensity indicates that some of silicate layers have disordered. On the contrary, MAPP/20A18 does not show any change of the peak position during heating and cooling but does show an increase in peak intensity on heating and a return to the exact initial value on cooling. The increase in peak intensity may be due to the fact that polymer crystallites disturbing the (001) reflection of silicate layers disappear during heating.

From the result of Figure 1, it is concluded that low angle peak of highly filled nanocomposites are originated from the ordering of silicate layers as wall as MAPE/20A18 experiences higher thermal expansion and faster disordering than MAPP/20A18 during thermal treatment. To preserve the shear-induced orientational structure of the silicate layers, all SAXS measurements were carried out at room temperature. The exact peak position of the nanocomposites was determined via the deconvolution procedure, as reported in a previous article.[31]

Figure 2a shows SAXS patterns of the MAPE/20A nanocomposites. The (001) reflection peak positions of layered silicate are pointed by the arrow symbol. SAXS patterns change with the silicate concentration. The (001) reflection peak is not shown below the concentration of 9 vol % but appears above 12 vol % silicate content. The peak becomes more intense as the concentration of silicate increases. Parts a and b of Figure 2 show SAXS patterns of MAPE/20A and MAPP/20A fibers with various amounts of silicates, which were scanned in the equatorial direction of fiber axis. The extruded MAPE/20A nanocomposite fibers show a more intensive and sharpened (001) reflection peak than the as-mixed MAPE/20A nanocomposites due to the orientation of the silicate layers in the flow direction. The former have almost the same peak position and pattern as the latter except for the nanocomposite with 9 vol % silicate content. The nanocomposite fiber with 9 vol % silicate shows the weak and broad (001) reflection peak around 0.5° after extrusion. It indicates that shear flow could induce the regular layered ordering of silicate layers in the nanocomposite.[34] In addition, MAPP/20A nanocomposite fibers show the similar SAXS patterns to MAPE/20A nanocomposite fibers.

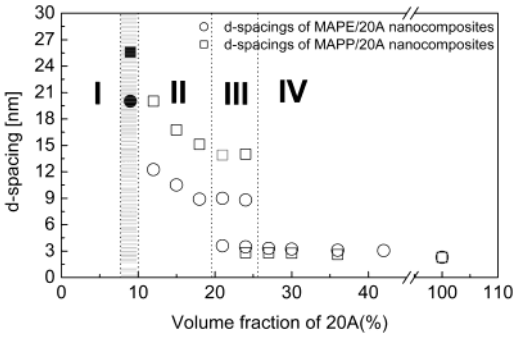

Figure 3. *d* spacings of the MAPE/20A and MAPP/20A nanocomposite fibers. Open circle symbol and open rectangular symbol indicate *d* spacings of MAPE/20A and MAPP/20A calculated from SAXS data, respectively. Solid symbols means *d* spacing created by shear-induced orientation.

Figure 3 shows the *d* spacings of the MAPE/20A and MAPP/20A nanocomposites. The *d* spacings are calculated by Bragg's law. Both nanocomposites show the similar *d* spacing dependency on the concentration of silicate. As reported previous article,[31] *d* spacings of both nanocomposites vary via four stages (I−IV) as a function of the concentration of silicate. In this article, we describe the morphology evolution from high concentration of silicate (stage IV) to low concentration (stage I) in order to understand clearly the process of the breaking-up of the multilayered silicate tactoid into separate individual layers. The *d* spacing of 20A is 2.4 nm. In stage IV, the *d* spacing of nanocomposites gradually increases as the concentration of silicate decreases. The increasing interlayer spacing is because polymer chains are intercalated into the interlayer space between silicate layers. The increasing the relative amount of polymer to silicate induces the increasing the interlayer spacing. The nanocomposites in this stage have intercalation morphology with the narrower layer spacing than 3.6 nm because of the high concentration of silicate. That is to say, in this stage, silicate layers interact strongly by van der Waals interactions as strong as they keep the intercalation morphology. In stage III, dual plane peaks are observed. One peak results from the wide *d* spacing of silicate layers and the other from the narrow *d* spacing. It indicates the coexistence of exfoliated and intercalated morphologies. The dual plane peaks in this stage provides the meaningful clue that the attractive interaction between silicate layers becomes dominant when the distance between them is smaller than a certain value as well as nanocomposites experiences the intercalation to

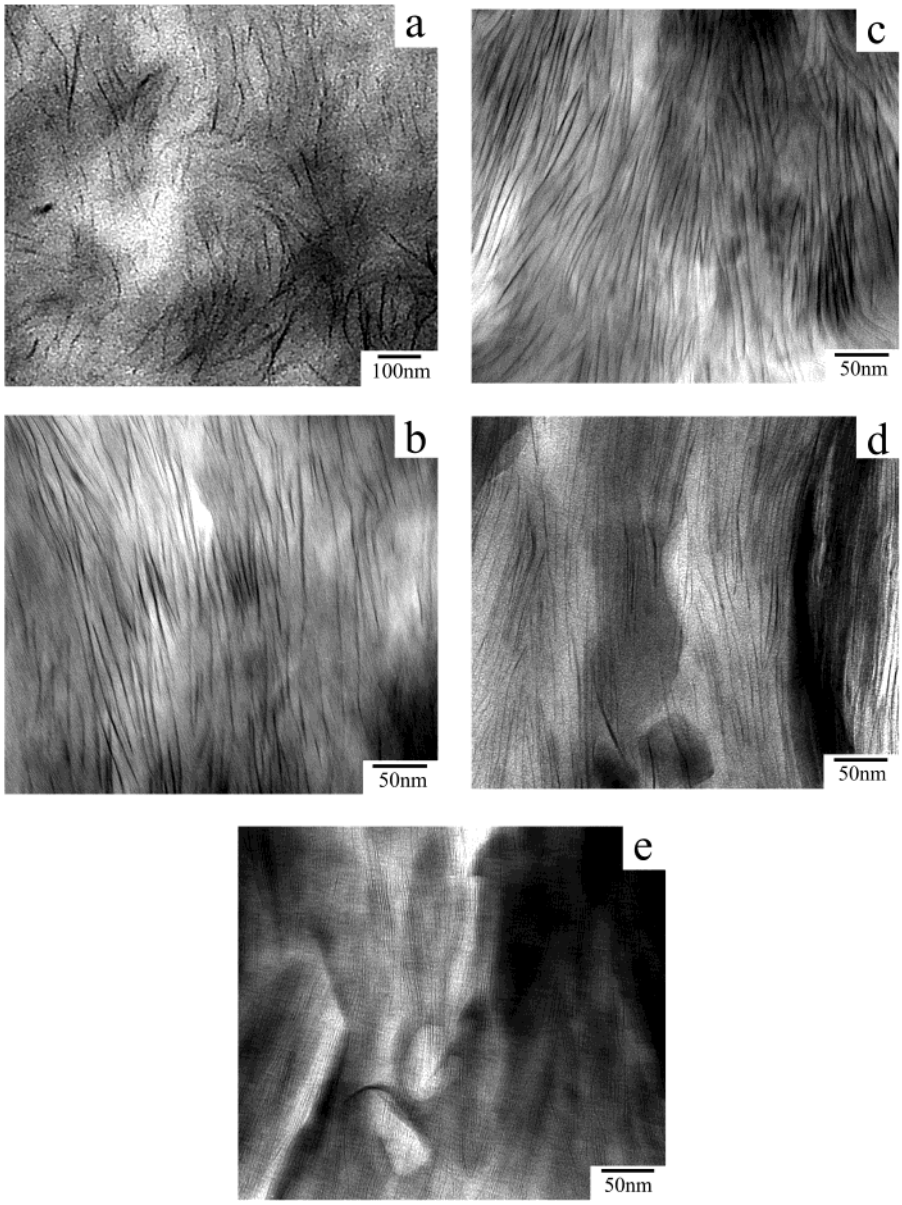

Figure 4. Transmission electron micrographs of MAPP/20A nanocomposite fibers with clay concentration of (a) 6, (b) 12, (c) 18, (d) 24, and (e) 36 vol %.

exfoliation morphology transition at a certain concentration region of silicates. As the concentration of silicate decrease from stage IV to stage III, the mean interlayer spacing may increase. Some of silicate layers can keep the wide interlayer spacing to be free from van der Waals attraction, not from steric interaction because silicate layers are quite long in length about a hundred nanometer. Therefore, in stage III, some portion of nanocomposites forms the exfoliation morphology and the other remains the intercalation morphology. From this result, it can be concluded that there is a critical distance between silicate layers, above which the favorable interaction between silicate layers and polymer chains overwhelms the attractive interaction between silicate plates. The critical distances of MAPE/20A and MAPP/20A are about 9 and 13 nm, respectively. In this stage, the wide and narrow *d* spacings are kept almost constant. As obviously shown in Figure 2b, the one peak with wide spacing gets weak and the other with narrow spacing becomes intense as the concentration of silicate increases. In stage II, MAPE/20A and MAPP/20A nanocomposites have wider layer spacings than 9 and 13 nm, respectively. Hence they have the ordered and exfoliated morphology. The layered regularity of the silicate layers in this stage must be from the steric interaction between silicate layers with the extremely high aspect ratio, not a particular interaction between silicate layers. The layer spacing gradually increases and the peak intensity of SAXS pattern gradually decreases as the concentration of silicate decreases. In stage I, periodicity of silicate layers is not observed. It means that individual silicate layer is randomly distributed. Because individual layers could keep the interlayer distance as far as they could not interact sterically. Therefore, the nanocomposites in this stage have the disordered and exfoliated morphology. Nevertheless, the artificially oriented extrudate would show the layer spacing if the interlayer distance exists within the detectable range as shown by the dark region between stages II and I in Figure 3.

Figure 4 shows typical transmission electron micrographs of MAPE/20A nanocomposites at each structural stage. An ultrathin film of MAPP/20A was prepared by

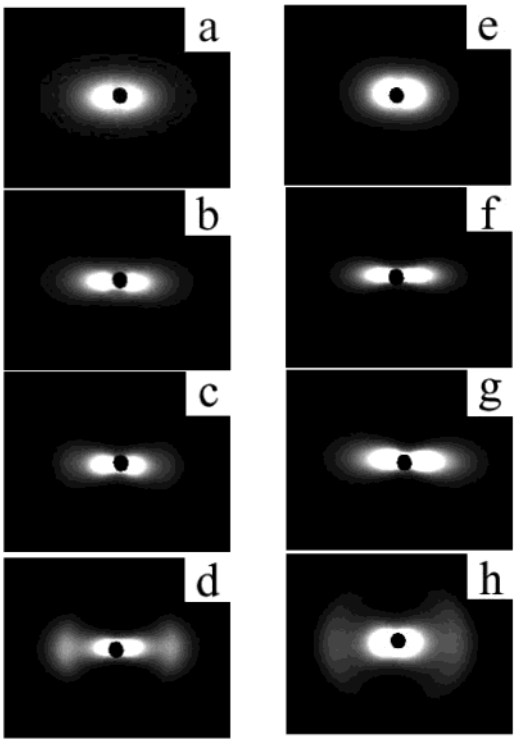

Figure 5. SAXS photographs of MAPE/20A nanocomposite fibers with clay concentration of (a) 6, (b) 12, (c) 24, and (d) 42 vol % and MAPP/20A nanocomposite fibers with clay concentration of (e) 6, (f) 12, (g) 24, and (h) 42 vol %, extruded at shear rate of 1000 s^{-1}. The nanocomposite fiber axis is laid in the meridian of the images.

slicing nanocomposites by cryogenic ultramicrotome at −120 °C. Dark lines in the images represent the silicate layers. Transmission electron micrographs of MAPE/20A were already reported in the previous paper.[31] MAPP/20A has the similar transmission electron micrographs with MAPE/20A over the whole concentration range of silicates. Silicate layers have a broad distribution in diameter ranging from 30 to 300 nm and the uniform distribution in thickness about 1 nm. Figure 4a shows the transmission electron micrograph of the 6 vol % MAPP/20A nanocomposite in stage I. One can see that individual silicate layers are well dispersed in the nanocomposites. Each silicate layer keeps the enough distance as far as they are free from steric hindrance from adjacent silicate layers. It shows disordered and exfoliated morphology. Parts a and b of Figure 4 show the transmission electron micrographs of MAPP/20A nanocomposites with 12 and 18 vol % silicate in stage II, respectively. In both photographs, it is observed that adjacent silicate layers are close enough to interact sterically within the distance smaller than an average length of silicates, forming the ordered and exfoliated structure in the polymer matrix. The mean layer spacings measured from TEM are about 13.0 nm comparable with the result of SAXS. Figure 4d shows the transmission electron micrograph of the MAPP/20A nanocomposite with 24 vol % silicate in stage III. As expected from Figure 3, two distinct regions can be observed. One region is a quite loose region in which layer silicates show an exfoliated morphology with the wider interlayer spacing than 13 nm. The other is a tightly stacked region in which layer silicates show an intercalated morphology with the narrower interlayer spacing than 3 nm. Figure 4e shows the MAPP/20A nanocomposite with 36 vol % silicates in stage IV. It shows the tightly stacked layer structure, which indicates a typical intercalated morphology. The results from transmission electron micrographs are well consistent with those from SAXS.

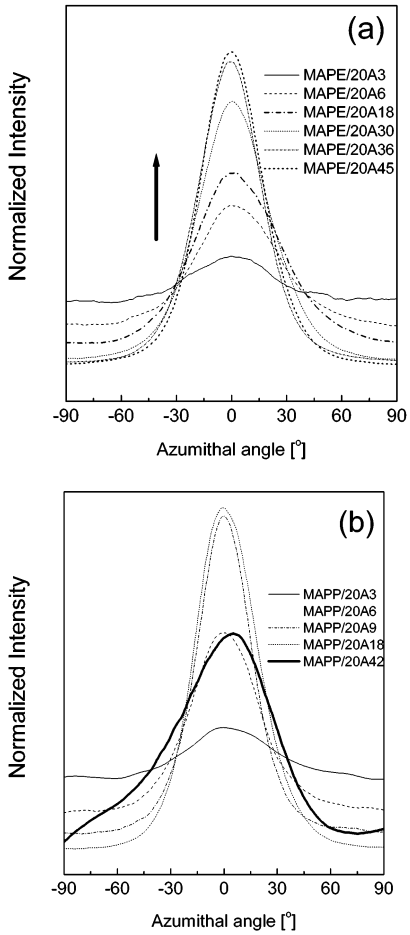

Figure 6. Normalized intensity of plane reflection of (a) MAPE/20A and (b) MAPP/20A fibers with angle ϕ between the platelets' normals and fiber axis.

Orientational Behaviors. Figure 5 shows the 2D SAXS photographs of MAPP/20A and MAPE/20A nanocomposite fibers extruded at shear rate 1000 s^{-1}. The nanocomposite fibers are laid in meridian direction. A reflection near the beam stopper is typical 2-D SAXS pattern of the exfoliated nanocomposite. A pair of reflections on the equator near the beam stopper appears in the intercalation, not in the exfoliation.[31,35−37] A precise relationship between morphology and 2D-SAXS photograph were reported previous paper.[31] The photographs of both nanocomposites show 2-D SAXS patterns agreeing well with their morphologies. In addition, they show the strongly anisotropic intensity distribution on the equator, which indicates that the silicate platelets' normals are oriented in the perpendicular direction to the flow direction. The degree of the order depends on the clay concentration as well as the type of nanocomposite.

Figure 6 shows the normalized intensity of plane reflection of MAPP/20A and MAPE/20A with angle ϕ between the platelets' normals and the flow gradient direction (radial direction of fiber). Actually, the total intensity means total reflection of layered silicates in the nanocomposites in the experimental SAXS range. The intensity at each angle is proportional to the amount of clay platelets aligned in each direction. The

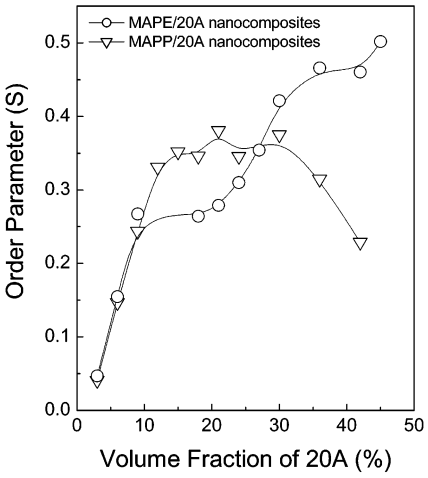

Figure 7. Order parameter (*S*) of (a) MAPE/20A and (b) MAPP/20A fibers with the concentration of silicates.

curves have been scaled by the silicate concentration to make them comparable to those of the more concentrated sample. Both nanocomposites show the Gaussian distribution with the center of $\phi = 0$, which indicate that the clay platelets' normals are aligned in the direction perpendicular to the flow direction. However, they show quite different shear-induced orientation behaviors with the concentration of silicates.

Figure 7 shows the order parameter (S) of MAPP/20A and MAPE/20A. The order parameter (*S*) was calculated from eq 1

$$S = \frac{3}{2}\langle \cos^2 \phi \rangle - \frac{1}{2} = \frac{\int_0^{90} I(\phi) \sin \phi \left(\frac{3}{2}\cos^2 \phi - \frac{1}{2}\right) \mathrm{d}\phi}{\int_0^{90} I(\phi) \sin \phi \, \mathrm{d}\phi} \tag{1}$$

Order parameter of MAPE/20A nanocomposites monotonically increases with the concentration of silicate. On the other hand, the order parameter of MAPP/20A nanocomposites increases with the clay loading up to an intermediate clay concentration and then decreases with the clay loading at the higher concentration. In the case of MAPE/20A nanocomposites, the monotonic increase of order parameter can be understood by the average effect of collisions between neighboring particles.[32,33] The collisions prevent the particles from tumbling freely and thus enhance the order. In the case of MAPP/20A nanocomposites, the gradual increase of order parameter at the low concentration of silicate must be from the average effect of collisions between neighboring particles. However, at the high concentration regime, the reason the order decreases is not easy to explain. The reduction of order at high concentration of silicates could be thought of as arising from three reasons.[32] The first reason may be due to the tumbling of domains. Tumbling of domains would be expected to reduce the orientational order. In intercalation morphology, tactoids consisting of several packed silicate layers may act as a domain as shown in Figure 4, parts d and e. The second reason may be due to the high viscosity of a highly concentrated dispersions. The dispersion of particles at a high concentration would require a greater shear force to achieve the same degree of order than that at a low concentration. It is called a highly effective thermal temperature.[38] The concept of effective thermal temperature has been described by

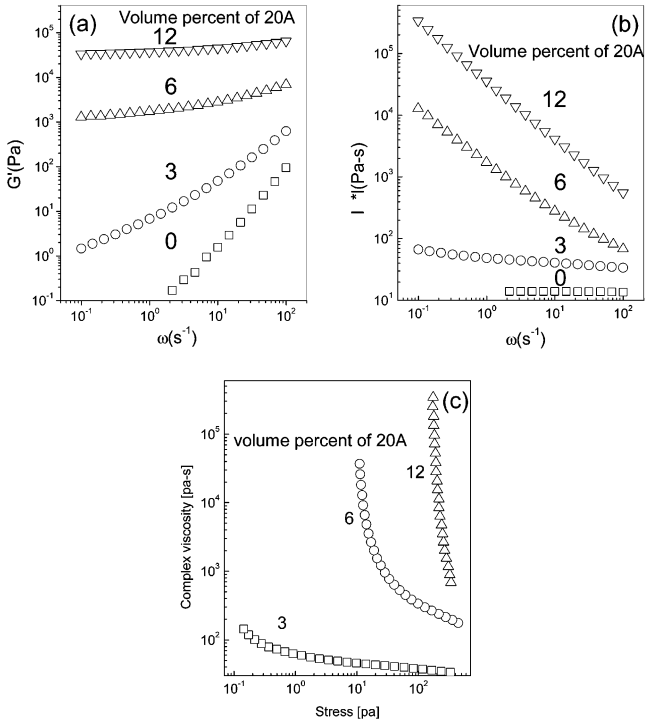

Figure 8. (a) Storage modulus, (b) complex viscosity vs shear rate, and (c) complex viscosity vs shear stress of MAPP/20A nanocomposites at 200°C.

Campbell[39] and Savage.[40] In a dilute system, the random movements of particles result from the thermal motion in the fluid, and so the effective temperature is simply the thermal temperature of the system. At a high concentration, collisions with neighboring particles induced by the shear of sample, could add the effective thermal energy to the particles. The third reason may be from the shear geometry.[41,42] The PLSN melt with yield stress may act like a Bingham fluid. When this kind of fluid flows through a tube, the core of the tube may have a plug flow and the boundary layer on the tube wall has a velocity gradient. The silicate layers are disordered in the core and may have orientation in the boundary region.

Figure 8 shows storage modulus, complex viscosity vs ω, and complex viscosity vs shear stress of MAPP/20A nanocomposites at 200 °C. We obtained data up to 12 vol % clay content for MAPP/20A above which stress overload occurred. The storage modulus and complex viscosity for all samples increase monotonically with the clay loading at all frequencies as expected by the filler effect and show a higher increase at the high frequency than at the low frequency. The terminal slopes of storage modulus also rapidly decrease as clay loading increases. Figure 8c shows a plot of complex viscosity vs stress in order to estimate the yield stress of the nanocomposites. MAPP/20A nanocomposites keep the constant stress with complex viscosity at the low frequency, namely yield stress. Yield stress increases sharply with silicate concentration.

Figure 9 shows the normalized intensity of plane peak of MAPP/20A36 and MAPE/20A36 with angle ϕ at various shear rates. MAPP/20A36 has a quite different intensity distribution from that of MAPE/20A36. In MAPP/20A36 the peak intensity decreases and the peak distribution broadens as the shear rate increases. On the contrary, In MAPE/20A36, the peak intensity increases and the peak becomes sharp with shear rate.

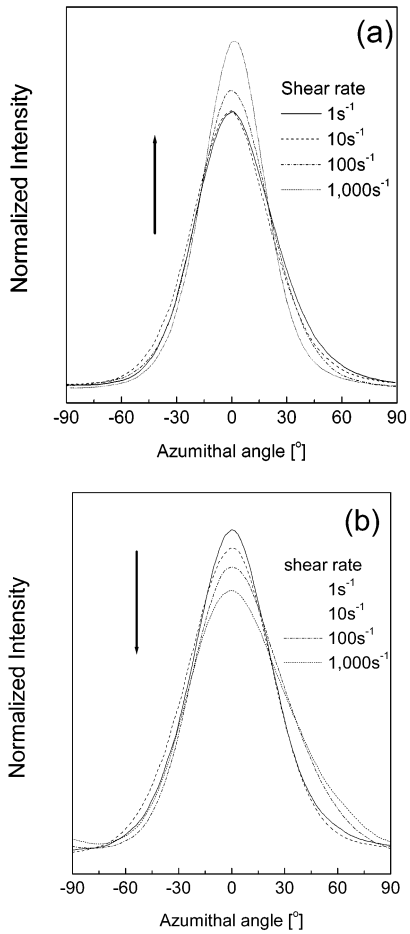

Figure 9. Normalized intensity of plane reflection of (a) MAPE/20A36 and (b) MAPP/20A36 fibers at various shear rates.

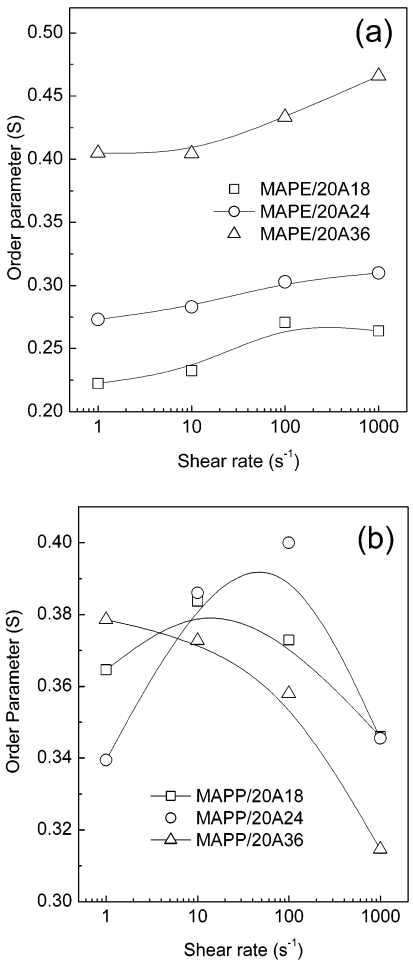

Figure 10. Order parameter (*S*) of MAPE/20A and MAPP/20A fibers with the silicate concentration of 18, 24, and 36 vol % at various shear rates.

Figure 10 shows order parameters of MAPE/20A and MAPP/20A with 18, 24, and 36 vol % silicates. All MAPE/20A nanocomposites show the monotonically increasing the degree of order with shear rate. On the other hand, MAPP/20A nanocomposites show the maximum and then the decrease in orientational order with the shear rate. The reduction of order in MAPP/20A would not be expected if the movements of the particles are taken as the effective thermal temperature and the plug flow.[38] The second reason is not applicable to MAPE/20A nanocomposites because the concept of effective thermal temperature expects the orientational order to increase with the shear rate.

In addition, the third reason is not applicable. As shown in Figure 8, the nanocomposites can be regarded as a Bingham fluid. For a Bingham fluid, the velocity gradient is zero when the momentum flux is less than the value τ_0. Hence one can expect a plug flow region in the central part of the tube, as described in Figure 11. The plug flow region with a radius r_0 is proportional to the yield stress (τ_0) according to eq 2.

$$r_o = \left(\frac{2\tau_0 L}{P_0 - P_L}\right) \tag{2}$$

The increase in yield stress with silicate concentration may seem to cause the ordering of MAPP/20A nanocomposites to reduce because of the wide plug flow region and the small boundary region on the tube wall with a velocity gradient. However, a plug flow cannot explain the reduction of the order of MAPP/20A with the shear rate because the higher shear rate induced by the higher pressure ($P_0 - P_L$) must generate the smaller plug flow region (r_0) by eq 2 and produces the higher orientational order. Therefore, the third reason must not be applicable to the MAPP/20A nanocomposites. Hence, the tumbling of tactoids in highly filled MAPP/20A nanocomposites may be the main cause observed to reduce the orientational order with the silicate concentration.

Figure 12 shows the transmission electron micrograph of the core part of MAPP/20A36 fiber. One can see several tactoids, which are made of several or several tens silicate layers. As expected, the tactoids show less aligned dispersion states. Some of them tumble clearly. Unexpectedly, one can see that lots of silicate layers are curved, especially in the end of tactoids. The clay layers known as a very rigid plate often show a curved structure in TEM due to their very large aspect ratio and nanometer thickness.[14] The easy curving behavior of silicate layers may facilitate the tumbling of tactoids in MAPP/20A nanocomposite with a high concentration of silicate. From Figures 9−12, it is concluded that the first reason may be the most applicable cause to the reduction of the order in the MAPP/20A nanocomposites. The outstanding tumbling effect in MAPP/20A may due to the fact that MAPP/20A has higher viscosity than MAPE/20A at this experiment condition, as reported in Figure 1 where MAPP/

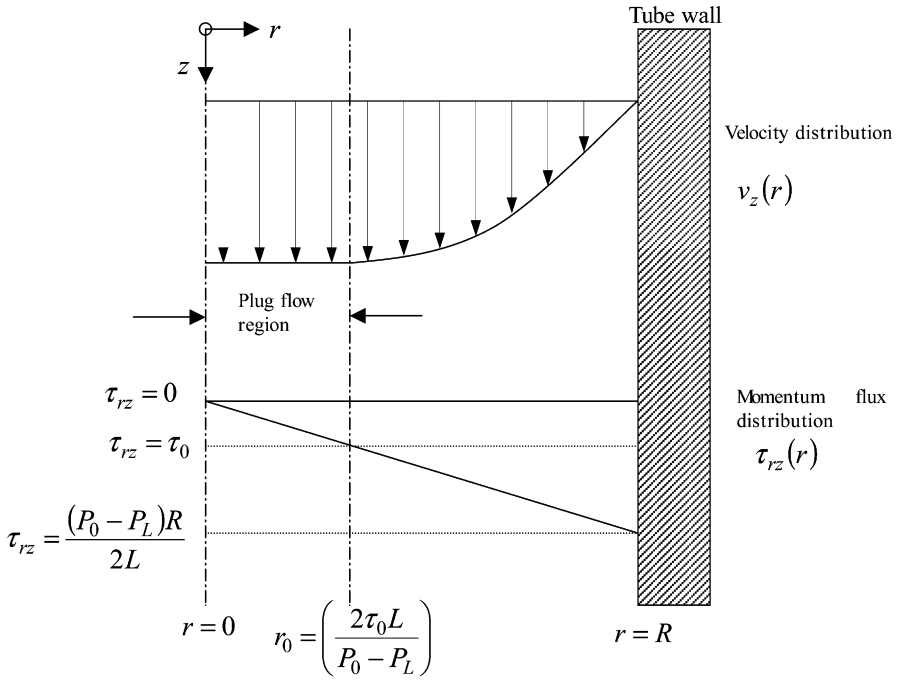

Figure 11. Schematic diagram of pipe flow of Bingham fluid. *R* is the radius and *L* is the length of the tube.

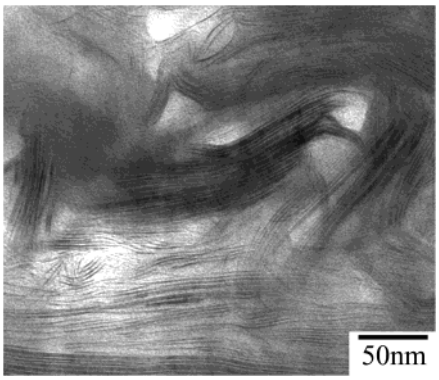

Figure 12. Transmission electron micrographs of the core of the MAPP/20A nanocomposite fibers with a clay concentration of 36 vol %.

20 needs much longer relaxation time than MAPE/20A at the same silicate concentration because MAPP/20A has the much higher viscosity.

Anisotropic Phase Formation of the Nanocomposite. Parts a−c of Figure 13 show polarized light micrographs of as-mixed MAPP/20A nanocomposites with 9, 12, and 18 vol % silicate at 200 °C, which is above MAPP melting temperature. Figure 13d shows a polarized light micrograph of extruded MAPP/20A nanocomposite fiber with 18 vol % silicate. The nanocomposites showed the darkness in the polarized light microscope up to 9 vol % silicate. Above 12 vol % silicate, birefringence appeared. Optical anisotropy becomes stronger with an increase in silicate concentration. MAPP/20A and MAPE/20A nanocomposites have the same isotropic to anisotropic transition concentration as reported in the previous paper.[31] The anisotropy must be originated from the ordered silicate plates in the flexible polymer of MAPP. It may mean that the self-assembled anisotropy of silicate layers starts to appear when the silicate concentration is higher than a certain critical concentration. The optically isotropic to anisotropic phase transition concentration of the nanocomposites are consistent well with the disordered exfoliation (stage I in Figure 3) to ordered exfoliation (stage II) transition concentration. The nanocomposite fiber in Figure 13d shows a more bright texture indicating a shear-induced optical anisotropy.

However, MAPE/20A and MAPP/20A nanocomposites did not exhibit a clear onset point of the biphasic region at which isotropic and anisotropic phases separate clearly. The texture did not show these two distinct domains. These observations may be from the high viscosity of the nanocomposites. In addition, the nanocomposite shows a shear-induced optical anisotropy near the isotropic to anisotropic phase transition concentration. Although the nanocomposite containing 9 vol % clay is not birefringent at rest, the extrudate displays strong anisotropy as reported in a previous paper.[31] In addition, the phase transition of both nanocomposites is athermal. The nanocomposites do not show any influence of temperature up to the degradation temperature of matrix polymers. In addition, the viscosity transition according to the concentration of silicate is not confirmed as shown in Figure 8. The apparent viscosity of both nanocomposites measured in the capillary flow increases almost exponentially with increasing clay concentration. The concentration at which the isotropic to anisotropic phase transition occurs, 12 vol % of silicates in nanocomposites, is quite higher than the simulated results, when a high aspect ratio of silicate layers about 100 is considered.[26−30] The reason is not clear. However, the large polydispersity of natural silicate plates in diameter and the existence of curved silicate layers as shown in TEM photographs, might cause the transition concentration to increase.

Conclusion

Morphology evolution, orientational behavior, and anisotropic phase formation of the maleated polyethylene-layered silicate nanocomposites and the maleated polypropylene-layered silicate nanocomposites were investigated. The final morphology of both polymer−silicate nanocomposites evolves via four stages; inter-

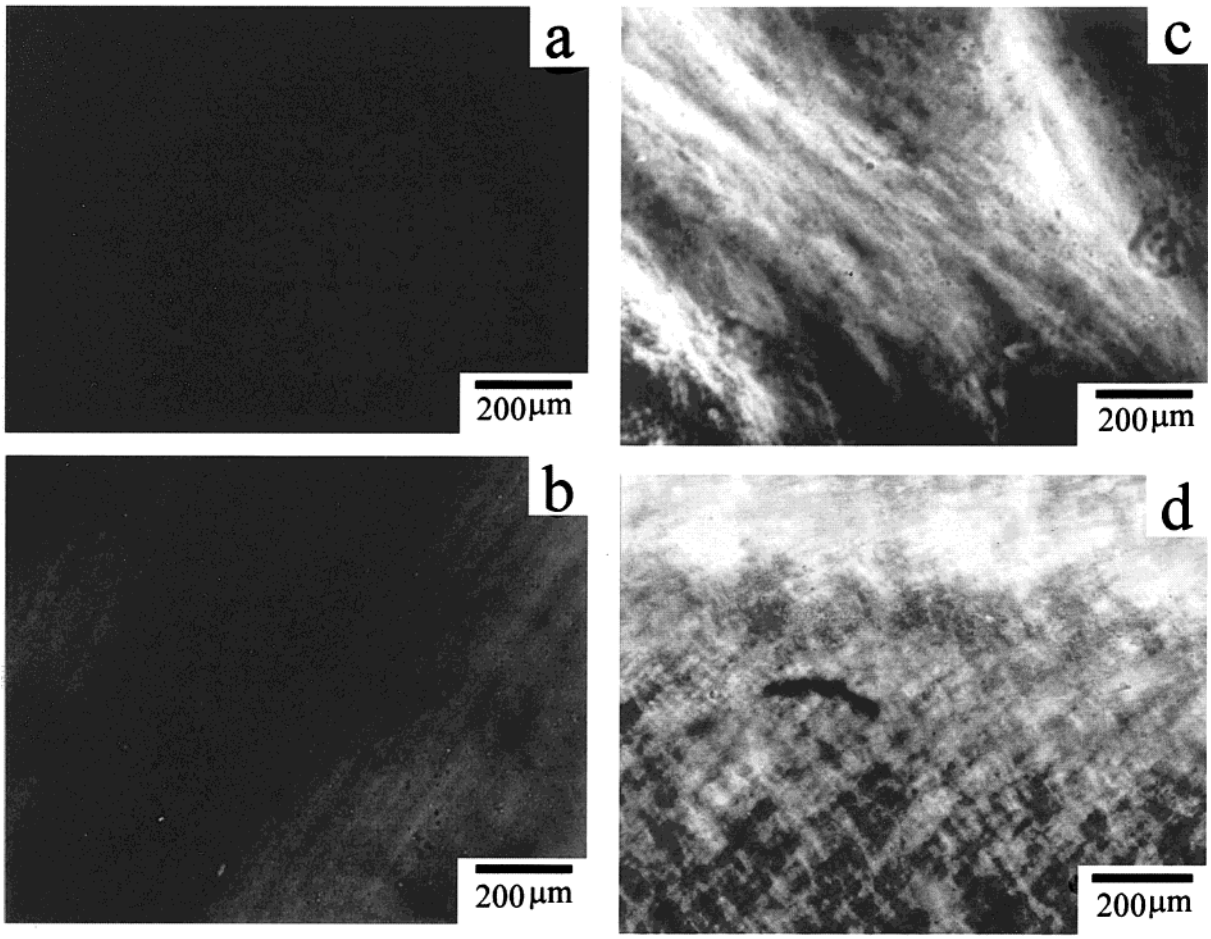

Figure 13. Polarized light micrographs of the as-mixed MAPP/20A nanocomposite with concentration of (a) 9, (b) 12, and (c) 18 vol % and the extruded MAPP/20A nanocomposite fiber with a concentration of (d) 18 vol %. Samples on the slide glass were squeezed very slowly with a cover glass to minimize the history of sample preparation at 200 °C. In particular, the extrudate was slightly squeezed to keep the sheared state.

calation, dual states of intercalation and exfoliation, ordered exfoliation, and disordered exfoliation in sequence as the concentration of silicate decreases. The morphology evolution of nanocomposites is determined by balancing the favorable interaction between polymer and silicate against interactions between silicate platelets such as a steric interaction and an attractive interaction, changing with the concentration of silicates. In particular, the existence of dual morphologies in stage III provides a clue to understanding the van der Waals attraction between adjacent layers in both nanocomposites. When the nanocomposite is sheared, the clay platelets' normals are aligned perpendicular to the fiber axis. Degree of orientational order changes with the concentration as well as shear rate in a complex manner. The extent of order is enhanced with the clay concentration. The enhancing orientational order with the clay concentration is due to increase of the collisions between particles. The collisions between particles prevent them from tumbling freely and thus enhance the order. Unexpectedly, the reduction of orientational order in highly concentrated MAPP/20A nanocomposites may be caused by the tumbling of tactoids. In addition, the ordering of silicate layers in the nanocomposite induces the optical anisotropy. From the microstructural point of view, the optically isotropic to anisotropic phase transition concentration of the nanocomposites are consistent well with the disordered exfoliation to ordered exfoliation transition concentration. MAPE/20A and MAPP/20A nanocomposites show the optical anisotropy above 12 vol % silicate.

Acknowledgment. This work was supported in part by Brain Korea 21 program and in part by the Center for Advanced Functional Polymers. We thank Doc. J. M. Park in Samsung General Chemicals for allowing the use of the cryogenic ultramicrotome and Doc. C. H. Kim in Honam Chem. Co. for providing the materials. Experiments at PLS were supported in part by MOST and POSCO.

References and Notes

(1) Kojima, Y.; Usuki, A.; Kawasumi, M.; Okada, A.; Fukushima, Y.; Kurauchi, T.; Kamigaito, O. *J. Mater. Res.* **1993**, *8*, 1185.
(2) Kojima, Y.; Usuki, A.; Kawasumi, M.; Okada, A.; Kurauchi, T.; Kamigaito, O. *J. Appl. Polym. Sci.* **1993**, *8*, 1185.
(3) Kawasumi, M.; Hasegawa, N.; Kato, M.; Usuki, A.; Okada, A. *Macromolecules* **1999**, *30*, 66333.
(4) Vaia, R. A.; Vasudevan, S.; Krawiec, W.; Scanlon, S. G.; Giannelis, E. P. *Adv. Mater.* **1995**, *7*, 154.
(5) Giannelis, E. P. *Adv. Mater.* **1996**, *8*, 29.
(6) Choi, M. H.; Chung, I. J.; Lee J. D. *Chem. Mater.* **2000**, *12*, 2977.
(7) Wang, K. H.; Choi, M. H.; Koo, C. M.; Chung, I. J. *Polymer* **2001**, *42*, 9819.
(8) LeBaron, P. C.; Wang, Z.; Pinnavaia, T. J. *Appl. Clay Sci.* **1999**, *15*, 11.
(9) Alexandre, M.; Dubois, P. *Mat. Sci. Eng.* **2000**, *28*, 1.
(10) Vaia, R. A.; Jandt, K. D.; Kramer, E. J.; Giannelis, E. P. *Macromolecules* **1995**, *28*, 8080.

(11) Hackett, E.; Manias, E.; Giannelis, E. P. *Chem. Mater.* **2000**, *12*, 2161.
(12) Bujdak, J.; Hackett, E.; Giannelis, E. P. *Chem. Mater.* **2000**, *12*, 2168.
(13) Vaia, R. A.; Sauer, B. B.; Tse, O. K.; Giannelis, E. P. *J. Polym. Sci.* **1997**, *35*, 59.
(14) Krishnamoorti, R.; Vaia, R. A.; Giannelis, E. P. *Chem. Mater.* **1996**, *8*, 1728.
(15) Krishnamoorti, R.; Vaia, R. A.; Giannelis, E. P. *Macromolecules* **1997**, *30*, 4097.
(16) Vaia, R. A.; Giannelis, E. P. *Macromolecules* **1997**, *30*, 8000.
(17) Lim Y. T.; Park, O. O. *Macromol. Rapid Commun.* **2000**, *21*, 231.
(18) Lim Y. T.; Park, O. O. *Rheol. Acta* **2001**, *40*, 220.
(19) Onsager, L. *Ann, N. Y. Acad. Sci.* **1949**, *51*, 627.
(20) Langmuir, I. *J. Chem. Phys.* **1938**, *6*, 873.
(21) Davidson, P.; Batail, P.; Gabriel, J. C. P.; Livage, J.; Sanchez, C.; Bourgaux, C. *Prog. Polym. Sci.* **1997**, *22*, 913.
(22) Gabriel, J. C. P.; Davidson, P. *Adv. Mater.* **2000**, *12*, 9.
(23) Gabriel, J. C. P.; Sanchez, C.; Davidson, P. *J. Phys. Chem.* **1996**, *100*, 11139.
(24) van der Kooij, F. M.; Kassapidou, K.; Lekkerkerker, H. N. W. *Nature* **2000**, *406*, 868.
(25) Lekkerkerker, H. N. W.; Stroobants, A. *Nature (London)* **1998**, *393*, 305.
(26) Lyatskaya, Y.; Balazs, A. C. *Macromolecules* **1998**, *31*, 6676.
(27) Balazs, A. C.; Singh, C.; Zhulina, E.; Lyatskaya, Y. *Acc. Chem. Res.* **1999**, *32*, 651.
(28) Ginzburg, V. V.; Balazs, A. C. *Macromolecules* **1999**, *32*, 5681.
(29) Ginzburg, V. V.; Singh, C.; Balazs, A. C. *Macromolecules* **2000**, *33*, 1089.
(30) Ginzburg, V. V.; Balazs, A. C. *Adv. Mater.* **2000**, *12*, 1805.
(31) Koo, C. M.; Ham, H. T.; Kim, S. O.; Wang, K. H.; Kim, D. C.; Zin, W. C. *Macromolecules* **2002**, *35*, 5116.
(32) Chen, G.; Liu, S.; Zhang, S.; Qi, Z. *Macromol. Rapid Commun.* **2000**, *21*, 746.
(33) Ogata, N.; Kawakage, S.; Ogihara, T. *J. Appl. Polym. Sci.* **1997**, *66*, 573.
(34) Jimenez, G.; Ogata, N.; Kawai, H.; Ogihara, T. *J. Appl. Polym. Sci.* **1997**, *64*, 2211.
(35) Kojima, Y.; Usuki, A.; Kawasumi, M.; Okada, A.; Kurauchi, T.; Kamigaito, O.; Kaji, K. *J. Appl. Polym. Sci. Polym. Phys.* **1995**, *33*, 1039.
(36) Brown, A. B. D.; Clarke, S. M.; Convert, P.; Rennie, A. R. *J. Rheol.* **2000**, *44*, 221.
(37) Jogun, S. M.; Zukoski, C. F. *J. Rheol.* **1999**, *43*, 847.
(38) Campbell, C. S. *Annu. Rev. Fluid Mech.* **1990**, *22*, 57.
(39) Campbell, C. S. *Annual Review of Fluid Mechanics*; Cambridge University Press: Cambridge, England, 1967.
(40) Savage, S. B. *Adv. Appl. Mech.* **1984**, *24*, 289.
(41) Hunter, R. J. *Foundations of Colloid Science: I*; Oxford University: New York, 1992.
(42) Hunter, R. J. *Foundations of Colloid Science: II*; Oxford University: New York, 1992.
(43) Bates, M. A.; Frenkel, D. *J. Chem. Phys.* **1998**, *109*, 6193.
(44) Bates, M. A.; Frenkel, D. *J. Chem. Phys.* **1999**, *110*, 6553.
(45) Bates, M. A. *J. Chem. Phys.* **1999**, *111*, 1732.
(46) Clarke, N.; Cuesta, J. A.; Sear, R.; Sollich, P.; Speranza, A. *J. Chem. Phys.* **2000**, *113*, 5817.

MA021377N